Emergency Radiology (2022) 29:809–817
https://doi.org/10.1007/s10140-022-02063-z

ORIGINAL ARTICLE

Efficacy of the scatter correction algorithm in portable chest radiography

Michael Lawson[1,2] · Lijun Qian[1] · Kenneth K. Lau[1,3] · Theo Lau[4] · David Massey[1] · Mohamed Badawy[1,5]

Received: 29 March 2022 / Accepted: 17 May 2022 / Published online: 25 May 2022
© The Author(s), under exclusive licence to American Society of Emergency Radiology (ASER) 2022

Abstract

Purpose Portable chest radiographs (CXRs) continue to be a vital diagnostic tool for emergency and critical care medicine. The scatter correction algorithm (SCA) is a post-processing algorithm aiming to reduce scatter within portable images. This study aimed to assess whether the SCA improved image quality (IQ) in portable CXRs.

Methods Objective and subjective IQ assessments were undertaken on both phantom and clinical images, respectively. For objective analysis, attenuators were placed on the anterior surface of the patient's thorax to simulate pathologies present within uniform regions of the phantom's lung and heart. Phantom CXRs were acquired with three different tube-current-times (mAs). Phantom images were processed with different SCA strengths. Contrast to noise ratios (CNR) within the attenuator were determined for each algorithm strength and compared to non-SCA images. For subjective analysis, two independent radiologists graded 30 clinical images with and without the SCA activated. The images were graded for IQ in different anatomical structures and overall diagnostic confidence.

Results Objectively, most strengths of the SCA improved the CNR in both regions. However, a detrimental effect was recorded for some algorithm strengths in regions of high contrast. Subjectively, both observers recorded the SCA significantly improved IQ in clinical CXRs in all anatomical regions. Observers indicated the greatest improvement in the lung and hilar regions, and least improvement in the chest wall and bone. All images with and without the SCA were deemed diagnostic.

Conclusion This study shows the potential radiation dose neutral IQ improvement when using an SCA in clinical patient CXRs.

Keywords Scatter correction · Portable chest radiography · Contrast to noise · Shimadzu Corporation

Introduction

Portable chest radiographs (CXRs) are crucial for in-patient imaging in hospitals [1]. The ongoing SARS-CoV-2 virus (coronavirus-19) pandemic has increased the use of portable radiography for acute care in some centers [2]. Provided images are acquired with acceptable image quality (IQ), performing portable CXRs at the patient's bedside has several advantages, including increased workflow efficiency [3] and patient acceptability [4], reducing the risk associated with

✉ Michael Lawson
lawson.michael9@gmail.com

Lijun Qian
Lijun.Qian@monashhealth.org

Kenneth K. Lau
Ken.lau.sh@gmail.com

Theo Lau
lau.theo@gmail.com

David Massey
David.Massey@monashhealth.org

Mohamed Badawy
Mohamed.badawy@monashhealth.org

1 Monash Imaging, Monash Health, Clayton, VIC 3168, Australia

2 Centre for Medical and Radiation Physics, School of Physics, Faculty of Engineering and Information Sciences, University of Wollongong, Wollongong, NSW 2500, Australia

3 Department of Medicine, Monash University, Clayton, VIC 3168, Australia

4 QScan Radiology Clinics, Aspley, QLD, Australia

5 Department of Medical Imaging and Radiation Sciences, School of Primary and Allied Health Care, Faculty of Medicine, Nursing and Health Sciences, Monash University, Clayton, VIC 3800, Australia

transporting critically unwell or immobile patients [5], and limiting infection transmission risk by minimizing the frequency of interactions between infectious patients and staff [6, 7].

As the result of photon-electron interactions, Compton scattered photons are redirected on a trajectory misaligned to the primary beam. While the probability of Compton scattering interactions in tissue remains relatively constant over the diagnostic energy range, the likelihood of photoelectric interactions decreases with photon energy, resulting in a relatively greater chance of scatter interactions [8]. The overwhelming majority of photons produced by general radiography X-ray tubes during portable chest X-rays are high energy [8], resulting in a scattered to primary ratio (SPR) of between 2 and 4; meaning 2–4 times as much scatter can reach the detector as primary beam when imaging through the thorax [9–11]. The SPR increases with increased tube voltage, greater patient thickness, and larger X-ray field sizes, all of which are routinely found in the chest, abdominal, and spinal X-ray imaging [12]. As the pixel values (PV) within an image comprises both primary and scattered photons [12], scattered radiation degrades contrast within an image by dispersing the photons over the image receptor, generating PVs which do not represent the level of absorption the primary beam has undergone.

Several prospective scatter reduction methods exist to combat the IQ degradation caused by scattered radiation, including decreasing tube voltage, collimating tightly to the region of interest, or implementing the "air-gap" technique or slit-scanning technologies. However, in most situations, these methods are practically difficult to implement in portable CXRs and are rarely used. More commonly, an anti-scatter grid is introduced between the patient and the image receptor, which attenuates scattered photons based on the photon's angle of incidence with the grid [13]. In this process, some primary beam photons are also attenuated by the interstitial or septal material [12]. Other drawbacks of anti-scatter grids include "grid cutoff" or artefacts resulting from stationary grids [14–16]. Imaging protocols involving a grid usually require the exposure parameters to be increased to compensate for the reduced number of photons reaching the detector [8]. The utilization of a grid in a CXR typically requires the dose to be increased by a factor of 2–3 [17]. Unsurprisingly, anti-scattered grid use for portable CXRs is inconsistent among sites [15, 18].

To overcome these practical constraints, several scatter correction post-processing algorithms (SCA) have been developed for use with portable radiography units, intending to reduce the effects of scattered radiation on IQ, including the Philips "Skyflow" [19–23], Fuji "Virtual Grid Software" [24–26], and Shimadzu SCA [27]. The detailed technical information in the Shimadzu SCA "White-Paper" is limited. However, the algorithm first requires a grid-less patient image acquired at a reference tube voltage (100 kVp). The algorithm then applies the predefined reconstruction kernel that estimates the scatter level within a grid-less patient image by comparing the pixel values within the patient image to an inbuilt object absent image acquired with the same exposure parameters. The estimated scatter contribution to the object absent image is then removed from the patient image, leaving the patient image where the scatter has been digitally suppressed [27].

Both "Skyflow" and "Virtual-Grid" software have been shown to improve the IQ in phantom and clinical images [19–26]. However, no studies assessing the efficacy of the Shimadzu SCA have been published. This study aimed to evaluate the efficacy of the Shimadzu SCA on imaging quality in phantom imaging and clinical CXRs.

Methods

Ethics

Local institutional low-risk ethics has been obtained (RES-21–0000-365Q).

Portable radiography unit

The portable X-rays were performed with the portable radiography unit Shimadzu Mobile Dart MX8, installed with proprietary SCA software (Shimadzu Corporation, Kyoto, Japan).

Objective image quality

Objective IQ was assessed using simulated radiographic acquisitions of a Kyoto Whole Body Adult PB-60 Phantom. The phantom's thorax contains several anatomically realistic organs, including the lungs with pulmonary vessels, trachea, heart, and liver with hepatic and portal veins. The thorax portion of the phantom was used to simulate an average-sized patient's portable CXR. Erect CXRs are most performed at our institution. Subsequently, the exposure conditions used in this study replicated local hospital protocols for erect portable AP CXRs performed on average-sized patients (100 kVp, and 180 cm source to image distance (SID)). The phantom was placed in the supine position, parallel to the floor, to allow for easier phantom alignment and created a replicable setup. During the first portion of acquired CXRs, two 1.5 cm × 1.5 cm × 1 mm of high purity (> 99.9%) aluminum attenuators were placed on the anterior surface of the phantoms chest to simulate low-contrast pathologies present within the chest. Due to its low effective atomic number, aluminum undergoes proportionally more Compton scattering interactions when compared to other attenuators

making aluminum ideal to assess changes in the presence of scatter within a reconstructed image. The reason for placing the aluminum attenuators on the anterior surface of the phantom's thorax was to generate the largest disbursement of scatter across the detector. The two attenuators were placed anterior to the lungs and heart regions over regions of uniform thickness and composition (Fig. 1a). The attenuator anterior to the lung was used to assess the algorithm's ability to enhance high contrast details, while the attenuator anterior to the heart was used to evaluate the algorithm's ability to enhance low-contrast details (Fig. 1b).

Patients of this phantom's size would typically undergo examinations at approximately 1.4–1.8 mAs at our institution. As such, images were acquired at three mAs settings (1 mAs, 1.4 mAs, and 1.8 mAs). The aluminum attenuators were then removed, and the acquisitions were repeated with the same exposure increments. Each attenuator and tube current combination was repeated three times (18 total acquisitions). Images acquired with the same exposure (mAs) and placement of aluminum attenuators were combined and constituted a "set."

The acquired raw images were each reconstructed with different SCA strengths enabled. The algorithm's strength refers to the degree of scatter reduction, with "10" corresponding to maximum scatter reduction and "0" indicating no post-processing scatter reduction. Raw images being reconstructed multiple times ensured any difference in the images could be attributed to the reconstructions themselves rather than the image acquisitions. Each raw image was reconstructed with five different strengths (90 total reconstructions). The algorithm strengths carefully chosen for analysis encapsulated the spectrum of the SCA capabilities, with the minimum (level 0), maximum (level 10), and intermediate (levels 2, 5 and 8) strengths selected.

The objective IQ was assessed by the contrast to noise ratio (CNR). CNR is considered an essential objective image metric and correlated with the visibility of objects within the image [28, 29]. To assess this, 225 mm^2 regions of interest (ROIs) were drawn inside the projection of two aluminum attenuators using ImageJ® (National Institute of Health, Maryland, USA). ImageJ calculated the mean pixel value (PV) and associated standard deviation (SD) within each of the ROIs. A script ensured that the location and size of each ROI was the same across each of the reconstructions. The mean PV and SDs were calculated from the distribution of PVs across the three images within the set.

To calculate CNR for a given mAs and algorithm strength, the set average PV of the images acquired with the aluminum attenuator was subtracted from the set average PV from the images acquired without the aluminum attenuator, divided by this set's SD. Each CNR was then normalized by the value calculated for the non-scatter-corrected image acquired at 1.4 mAs. This value was selected as it most closely mimics the exposure and reconstruction parameters used in clinical practice for a patient of the phantom's size.

Subjective image quality

Thirty consecutive adult portable chest X-rays performed in the emergency department, which utilized anti-scatter correction from the Shimadzu Mobile DaRt unit, were included. Images containing motion artifacts, an incomplete field of view, or pediatric studies were excluded. All included studies were acquired using the "Chest Lscape AP Scatter Correction 100kVp" protocol and at variable, mAs based on patient habitus. All thirty images were performed at approximately 180 cm source to image distance (SID). A "level 5" scatter

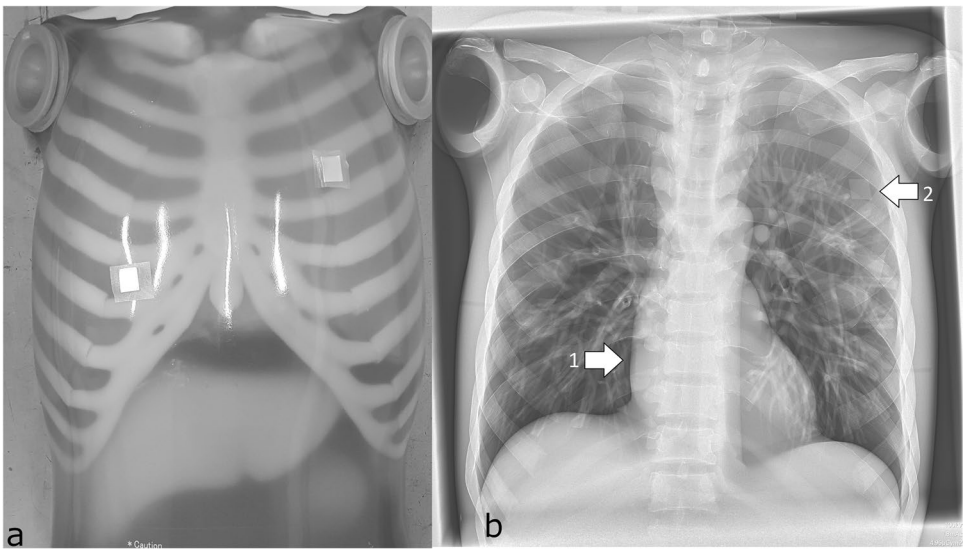

Fig. 1 **a** Placement of the aluminum attenuators on the surface of the PBU-60 phantom (white vertical lines are reflection of shiny surface of the phantom). **b** Appearance on radiographic acquisition (arrow 1 showing the low-contrast attenuator over the phantom's right heart border, arrow 2 showing the high contrast attenuator over the phantom's left lung)

correction was implemented based on results found in the objective portion of the study and after discussions with Senior Radiologists. It also reflected an intermediate level between high noise/high contrast and low noise/low contrast within the images. The same 30 image data sets were then reprocessed without the SCA by unselecting the "Scatter Correction" checkbox in the image's reconstruction properties. As a result, 60 de-identified CXR images in total were created. Therefore, the images processed under the "no" SCA also had the same kV, mAs, and SID parameters. This meant images were obtained with the SCA and then retrospectively had the correction turned off accurately represented how the images would have appeared if the images were acquired without the algorithm selected during acquisition.

Table 1 indicates the patient characteristics and study indications. Patients presented with a diverse range of physical features and clinical indications.

Two radiologists with 31 years and 7 years of plain radiography experience independently reviewed all 60 images in the same randomized order. The reviewers were blinded to which images had the SCA applied. The observers studied one image at a time on the standard Picture Archiving and Communication System (PACS) to prevent bias. Both observers viewed the images under the same lighting conditions on monitors that met the performance requirements for general radiography reporting [30]. The reviewers graded the overall IQ (contrast, noise, and perceived resolution) of the lung, hilar, mediastinum, pleural cavity, bone, and chest wall on a 5-point Likert scale which covers most of the anatomical structures on chest radiography. Additionally, each observer also graded the overall diagnostic confidence as either "confident" or "not confident" based on the observers' ability to diagnose the images.

Table 1 Patient characteristics

Patient characteristic ($N=30$)	Median (25th–75th percentile)
Age (years)	68 (59–78)
Weight (kg)	68.4 (60–95)
Male (%)	50%
Referral reasons/clinical indications	
Cause of shortness of breath	10 (33%)
Lower respiratory tract infection	4 (13%)
Pneumonia	3 (10%)
Acute pulmonary edema (APO)	3 (10%)
COVID-19	3 (10%)
Chest pain for cause	3 (10%)
Chest infection	3 (10%)
Lung cancer and metastasis	3 (10%)
Congestive cardiac failure (CCF)	2 (7%)
Pulmonary embolism (PE)	2 (7%)
Septic screen	1 (3%)
Chest sepsis	1 (3%)
Delirium screen	1 (3%)
Chronic obstructive pulmonary disease (COPD)	1 (3%)
Consolidation	1 (3%)

Statistical analysis

The Cohen's kappa statistic with a 95% confidence interval (CI) was employed to assess the inter-observer reliability between observer 1 and observer 2 for each category. The inter-observer effect size was determined against the Koch and Landis criteria [31]. Values equal to 0 indicate no agreement, 0.01–0.20 as none to slight, 0.21–0.40 as fair, 0.41–0.60 as moderate, 0.61–0.80 as substantial, and 0.81–1.00 as almost perfect agreement.

The median and range were calculated based on combined scores from both observers. A Mann–Whitney *U* test with a 95% CI was employed to determine whether a statistical difference in IQ existed between the scatter-corrected and non-scatter-corrected images for each anatomical location.

Results

Objective image quality

Figures 2 and 3 show the normalized CNRs for the aluminum attenuators anterior to the lung (high-contrast enhancement) and the heart (low-contrast enhancement) region of the phantom. Both figures show higher relative CNRs for image sets acquired at greater mAs. Figure 2 show the selected algorithm strengths improved the CNR of the high contrast object for most mAs settings, with only "level 8" and "level 10" algorithm strengths degrading the CNR at the two lowest tube current–time settings. "Level 5" provided the greatest CNR enhancement, with an approximately 3% increase when compared to the non-scatter-corrected image across all mAs settings. Figure 3 shows the contrast of the attenuator in the (low contrast) heart region. Figure 3 indicates the greatest relative CNR enhancement was achieved using algorithm "level 10" and the lowest relative CNR was noted for images that had not been scatter-corrected. The SCA "level 2," "level 5," "level 8," and "level 10" elevated the relative CNR within the low-contrast-attenuator by an average of 10%, 15%, 23%, and 32%, respectively, across each of the tube voltages. Figure 3 also indicates a higher relative CNR for all algorithm strengths at 1.4 mAs when compared to the relative CNR of images acquired at 1.8 mAs without the scatter correction applied.

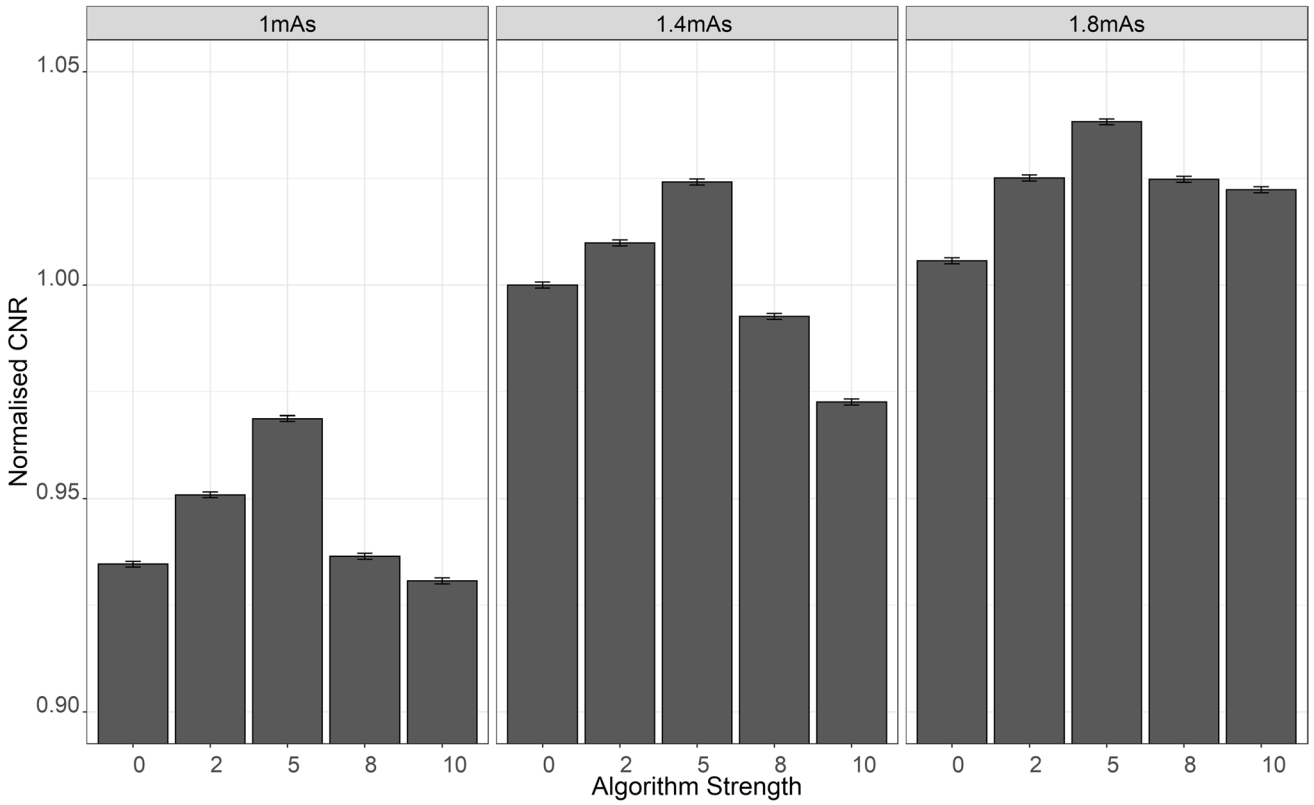

Fig. 2 Relative CNR as a function of algorithm strength and mAs for high contrast attenuator

Subjective image quality comparison

Interobserver agreement

Table 2 indicates high interobserver agreement levels in scores provided for different regions by the two observers. When graded against the Koch and Landis criteria, all regions had a "substantial" level of interobserver agreement.

Subjective image quality analysis

A series of Mann–Whitney *U* tests showed the scatter-corrected images received statistically significantly higher ratings (Table 3). As noted in the mean rank and U-statistics, the observers recorded the SCA had the largest improvement in IQ in the mediastinum and lung regions. Bone and hilar regions were recorded as the lowest areas of improvement. All images with and without the SCA were considered diagnostically adequate for both reviewers to make an accurate diagnosis and were without image artifacts (Fig. 4).

Table 4 presents the IQ changes in individual anatomical parts by comparing the scatter-corrected image to the non-scatter-corrected image of each patient. An "improved" IQ for a given region was defined as a higher rating attributed to the scatter-corrected image than the matching non-scatter-corrected image. Similarly, a "reduced" image was defined as the scatter-corrected image attributed with a lower rating than the non-scatter-corrected image. The SCA improved the overall subjective contrast, noise, and perceived resolution across all anatomical regions in 50% of the images. The SCA only reduced subjective IQ in the lung, hilar, mediastinum, and chest wall in less than 2% of images and bone and pleural regions in less than 7% of cases.

Discussion

The ongoing COVID-19 pandemic poses a significant challenge to frontline health networks. Portable CXRs allow increased patient throughput and minimize the chance of virus spread during patient transit to the radiology department [7]. It offers a more feasible alternative for critically unwell patients. However, this increased uptake of portable CXRs puts increased focus on optimizing imaging, particularly IQ.

IQ refers to the exactness with which objects or structures are reproduced on a radiographic image. In chest

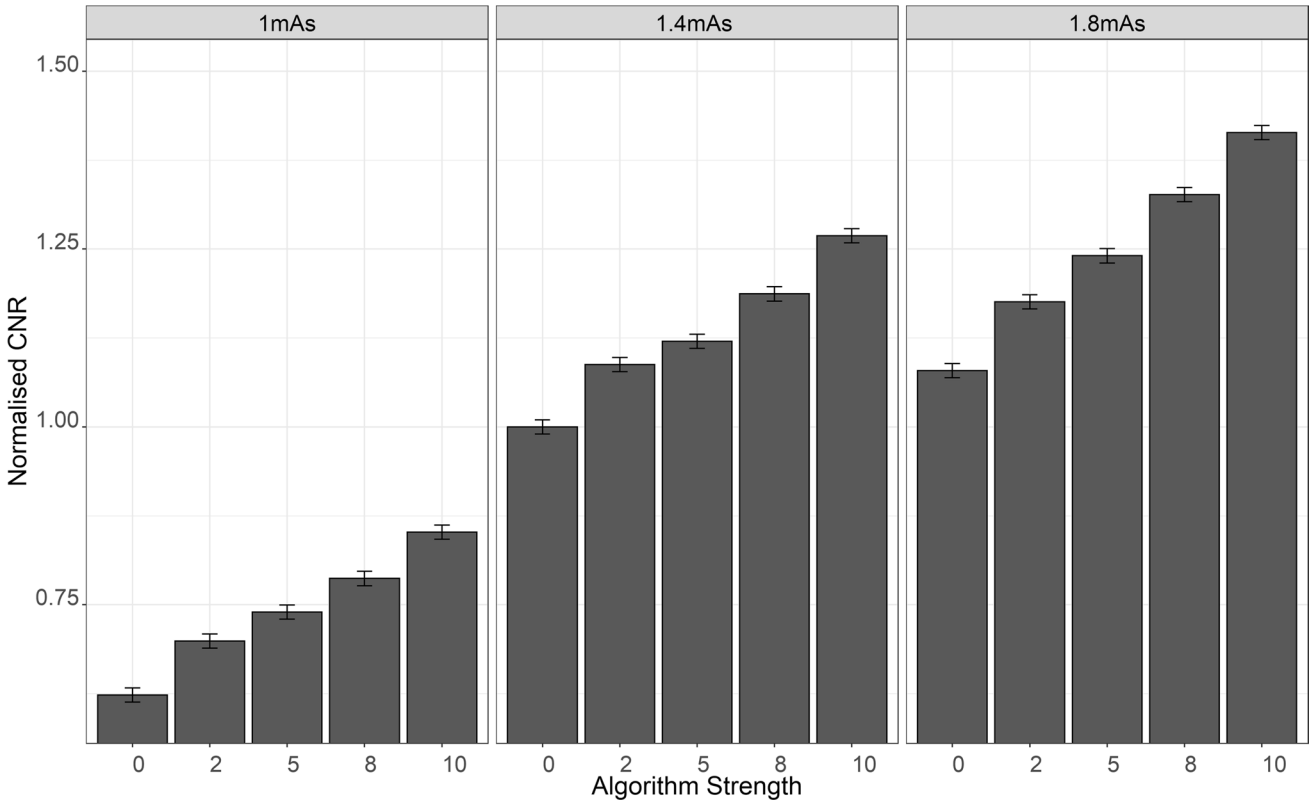

Fig. 3 Relative CNR as a function of algorithm strength and mAs for low contrast attenuator

Table 2 Cohen's kappa statistic for interobserver agreement for all anatomical regions

Region	Kappa value
Lung	0.67
Pleural	0.74
Mediastinum	0.69
Pleural	0.62
Bone	0.65
Chest wall	0.62

radiographs, IQ refers to the ability to depict all anatomical structures clearly and accurately within the image, such as the lung, hilar, mediastinum, pleural, bone, and chest wall, and interpret any disease or pathology associated with these structures. Higher IQ typically allows for a more confident clinical diagnosis, which can impact the patient's level of care. This study is the first to assess, objective or subjectively the impact of the Shimadzu SCA on IQ.

Table 3 Mann–Whitney *U* test of the non-scatter-corrected and scatter-corrected images

Anatomical region	Group	*n*	Mean rank	*U*	*z*	*p*
Lung	Non-scatter	60	42.93	746.00	−5.92	< .001
	Scatter	60	78.07			
Hilar	Non-scatter	60	45.94	926.50	−5.22	< .001
	Scatter	60	75.06			
Mediastinum	Non-scatter	60	42.73	733.50	−6.04	< .001
	Scatter	60	78.28			
Pleural	Non-scatter	60	44.44	836.50	−5.54	< .001
	Scatter	60	76.56			
Bone	Non-scatter	60	47.16	999.50	−4.69	< .001
	Scatter	60	73.84			
Chest wall	Non-scatter	60	43.23	764.00	−5.97	< .001
	Scatter	60	77.77			

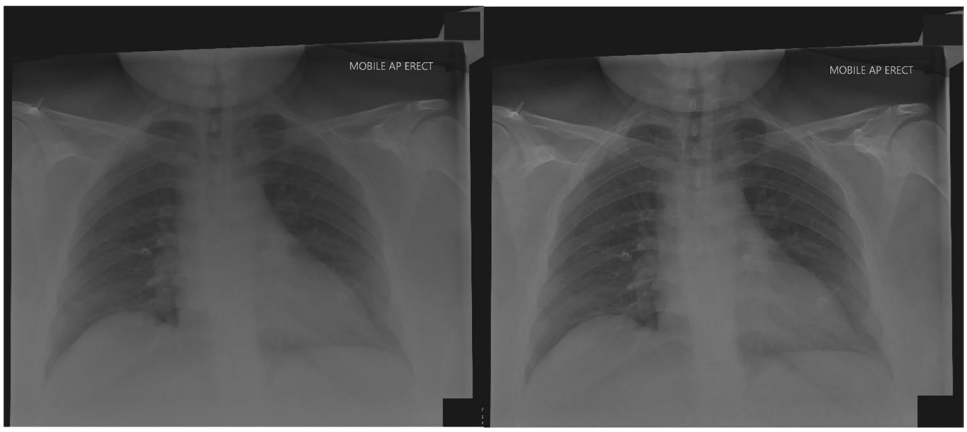

Fig. 4 Mobile digital frontal chest radiograph of a 27-year-old obese female patient demonstrated better demarcation of pulmonary vessels and hilar structures, and sharper interfaces of mediastinal/lung and lung/bone interfaces despite the body habitus on the image with SCA (right) as compared to the image without SCA (left)

Table 4 The change in IQ across included studies with the SCA applied for each region in %

	Lung	Hilar	Mediastinum	Pleural	Bone	Chest wall
Improved	68	55	72	67	50	57
Neutral	30	43	26	26	43	41
Reduced	2	2	2	7	7	2

Both objective and subjective assessments indicated improved IQ of structures within radiographs utilizing the SCA. Objectively, the SCA algorithm increased the relative CNR for both measurement positions and across most mAs and algorithm strengths. This is likely attributed to the increased contrast instigated by the subtraction of scattered radiation within the phantom image. This contrast increase had the greatest benefit in the low-contrast cardiac region, where the difference in PV between the attenuator and the background was minimal. For the high-contrast attenuator superimposing the lung, the relative CNR increase was more modest, with level 5 increasing the relative CNR by an average of 3% compared to images reformatted without the SCA. "Level 8" and "level 10" were shown to have a detrimental effect on the CNR at low mAs values in regions of high contrast. This may be due to an enhancement of noise within the ROI, which was not proportional to the increase in contrast. However, "level 8" and "level 10" SCA strength provide positive CNR enhancement when utilizing a higher dose (1.8 mAs) acquisition. A greater enhancement of low contrast pathologies has also been noticed in other objective studies evaluating Philips Skyflow [32].

Subjectively, both observers agreed the SCA enhanced the overall IQ, contrast, noise, and apparent resolution in all anatomical regions of clinical patient CXRs, and they did not comment on any detrimental effect from significant image noise or artifacts. While the level of improvement was variable across anatomical parts, the SCA improves the lung and mediastinum in over 68% of scores. The hilar, pleural, bone and chest wall scores increased in 55%, 67%, 50%, and 57% of image sets, respectively. In less than 2% of images, there was an IQ reduction in the lung, hilar, mediastinum, and chest wall. In 7% of scores, one reviewer indicated the bone and pleural regions exhibited a reduction in IQ after applying the SCA; however, this IQ reduction was not indicated in the second reviewers scores. The impact of SCA on the IQ improvement on the bony regions was the least amongst all anatomical parts, which was likely due to the algorithm being based on the scattering properties of soft tissue and not bone. Also, due to a higher atomic number and a lower relative electron density associated with bone, proportionately fewer photons undergo Compton scattering when passing through, resulting in bone having a lower impact on the scatter and, therefore, less affected by the algorithm.

While it was determined the SCA increased the overall IQ of the clinical portable CXRs, it was also noted that all images within the non-scatter-corrected image set were of adequate diagnostic quality. The objective analysis indicated the SCA improved relative CNR within the attenuators. Figures 2 and 3 indicate a greater relative CNR was achieved for both attenuators when images were acquired with 1.4 mAs and reconstructed with a SCA strength of "level 5" compared to images acquired with a 1.8 mAs exposure without SCA reprocessing. This finding suggests that images utilising the SCA could be performed with a lower mAs [17], reducing the patient's radiation exposure, and decreasing their theoretical stochastic risk [33]. Extrapolating such a dose reduction for all patients who receive portable CXRs would result in a substantial cumulative dose reduction to patients and staff tasked with performing the portable CXRs. However, a prospective study is required to confirm these findings.

This research has several limitations which should be considered in future research. This study only assessed the results of the algorithm at a single institution with a small number of patients in the subjective assessment. Other institutions may have different imaging protocols, impacting the SCA's effect in the clinical images. Future studies assessing the SCA should evaluate its potential use in other anatomical regions such as the abdomen. Furthermore, despite this study indicating the SCA has provided an overall improvement for all patients within the present cohort, the level of improvement will likely vary across patient habitus sizes, particularly for patients with less typical physiques. Additionally, the objective analysis performed in this study was limited to a single phantom size. Therefore, future studies may aim to determine whether optimization is possible by adjusting SCA algorithm strengths based on the patient's physical characteristics and whether the SCA is feasible for use in pediatric patients.

Conclusion

This study is the first to assess the effect of the SCA on the IQ of portable CXRs. Both objective and subjective measures showed the SCA improved the overall IQ of the portable CXR without increasing the patient's radiation dose. The SCA significantly enhanced the overall IQ of all anatomical structures for various patient sizes and pathologies.

Declarations

Conflict of interest The authors declare no competing interests.

Ethical approval This study has been reviewed by the local institutions ethical review board. Low-risk ethics has been granted for this project.

References

1. Brainsky A, Fletcher RH, Glick HA, Lanken PN, Williams SV, Kundel HL (1997) Routine portable chest radiographs in the medical intensive care unit: effects and costs. Crit Care Med 25(5):801–805
2. P. Yeung, J.-A. Pinson, M. Lawson, C. Leong, and M. K. Badawy, "COVID-19 pandemic and the effect of increased utilisation of mobile X-ray examinations on radiation dose to radiographers," *J. Med. Radiat. Sci.*, vol. N/A, no. N/A, 2022.
3. Kjelle E, Lysdahl KB (2017) Mobile radiography services in nursing homes: a systematic review of residents' and societal outcomes. BMC Health Serv Res 17(1):1–8
4. C. A. for D. and T. in Health, "Portable versus fixed X-ray equipment: a review of the clinical effectiveness, cost-effectiveness, and guidelines [Internet]," *URL https//www. cadth. ca (дата обращения 22.02. 2016)*.
5. Korner M, Weber CH, Wirth S, Pfeifer K-J, Reiser MF, Treitl M (2007) Advances in digital radiography: physical principles and system overview. Radiographics 27(3):675–686
6. Wu G, Li X (2020) Mobile X-rays are highly valuable for critically ill COVID patients. Eur Radiol 30:5217–5219
7. Brady Z et al (2020) Technique, radiation safety and image quality for chest X-ray imaging through glass and in mobile settings during the COVID-19 pandemic. Phys Eng Sci Med 43(3):765–779
8. Barnes GT (1991) Contrast and scatter in x-ray imaging. Radiographics 11(2):307–323
9. Miettunen R, Korhola O, Savikurki S (1991) The scatter-to-primary ratio as a function of varying X-ray absorption measured by computed radiography. Eur J Radiol 13(2):156–159
10. Niklason LT, Sorenson JA, Nelson JA (1981) Scattered radiation in chest radiography. Med Phys 8(5):677–681
11. Morneburg H (1995) Bildgebende Systeme für die medizinische Diagnostik: Röntgendiagnostik und Angiographie, Computertomographie, Nuklearmedizin. Sonographie, integrierte Informationssysteme. Publicis MCD-Verlag, Magnetresonanztomographie
12. Aichinger H, Dierker J, Joite-Barfuß S, Säbel M (2004) "Scattered radiation," in Radiation exposure and image quality in X-ray diagnostic radiology, Springer, pp. 45–56
13. Neitzel U (1992) Grids or air gaps for scatter reduction in digital radiography: a model calculation. Med Phys 19(2):475–481
14. Akhtar W, Aslam M, Ali A, Mirza K, Ahmad N (2008) Film retakes in digital and conventional radiography. J Coll Physicians Surg Pakistan 18(3):151
15. Anderson DW (2006) Introduction of grids to mobile ICU radiography in a teaching hospital. Br J Radiol 79(940):315–318
16. O'Donovan PB, Skipper GJ, Litchney JC, Salupo AJ, Bortnick JR (1992) Device for facilitating precise alignment in bedside radiography. Radiology 184(1):284–285
17. Uffmann M, Schaefer-Prokop C (2009) Digital radiography: the balance between image quality and required radiation dose. Eur J Radiol 72(2):202–208
18. Martin CJ (2007) "Optimisation in general radiography". Biomed Imaging Interv J 3(2)
19. P. SkyFlow, "Grid-like contrast enhancement for bedside chest radiographs acquired without anti-scatter grid."
20. Lisson CG et al (2020) Improvement of image quality applying iterative scatter correction for grid-less skeletal radiography in trauma room setting. Acta radiol 61(6):768–775
21. Lisson CG, Lisson CS, Kleiner S, Regier M, Beer M, Schmidt SA (2019) Iterative scatter correction for grid-less skeletal radiography allows improved image quality equal to an antiscatter grid in adjunct with dose reduction: a visual grading study of 20 body donors. Acta radiol 60(6):735–741
22. Renger B et al (2016) Evaluation of dose reduction potentials of a novel scatter correction software for bedside chest x-ray imaging. Radiat Prot Dosimetry 169(1–4):60–67
23. Precht H et al (2019) Can scatter correction software replace a grid in DR pelvic examinations? Radiat Prot Dosimetry 187(1):8–16
24. Suzuki R, Goto T, Ogawa H, Amimoto N (2016) "Evaluation of no-grid radiography using the digital scattered x-ray removal processing"
25. Kawamura T, Naito S, Okano K, Yamada M (2015) Improvement in image quality and workflow of x-ray examinations using a new image processing method, 'Virtual Grid Technology.' Fujifilm Res Dev 60:21–27
26. Gossye T, Smeets PV, Achten E, Bacher K (2020) Impact of software parameter settings on image quality of virtual grid processed radiography images: a contrast-detail phantom study. Invest Radiol 55(6):374–380
27. Go YS, Takayanagi, Hiroshi, Miyata, Keita Goto, T. M. Toma Hirai, Takashi Sasaki, Junya Yamamoto, K. H. Kazuyoshi Nishino, Masaaki Shibata, and and R. T. Yoshinori Ohno, Tetsuya Kobayashi (2017) "Development of scatter correction software," Kyoto, Japan, 1

28. Keenan HT, Runyan DK, Marshall SW, Nocera MA, Merten DF, Sinal SH (2003) A population-based study of inflicted traumatic brain injury in young children. JAMA 290(5):621–626
29. Doyle P, Martin CJ, Gentle D (2006) Application of contrast-to-noise ratio in optimizing beam quality for digital chest radiography: comparison of experimental measurements and theoretical simulations. Phys Med Biol 51(11):2953
30. Bevins NB, Silosky MS, Badano A, Marsh RM, Flynn MJ, Walz-Flannigan AI (2020) Practical application of AAPM Report 270 in display quality assurance: a report of Task Group 270. Med Phys 47(9):e920–e928
31. Landis JR, Koch GG (1977) "The measurement of observer agreement for categorical data". Biometrics 159–174
32. Mentrup D, Jockel S, Menser B, Neitzel U (2016) Iterative scatter correction for grid-less bedside chest radiography: performance for a chest phantom. Radiat Prot Dosimetry 169(1–4):308–312
33. Ulanowski A, Kaiser JC, Schneider U, Walsh L (2020) "Lifetime radiation risk of stochastic effects–prospective evaluation for space flight or medicine". Ann ICRP 49(1_suppl):200–212

Publisher's note Springer Nature remains neutral with regard to jurisdictional claims in published maps and institutional affiliations.